

# GTA: Advancing Image-to-3D World Generation via Geometry Then Appearance Video Diffusion

Hanxin Zhu<sup>1</sup>, Cong Wang<sup>2,3</sup>, Peiyan Tu<sup>2,5</sup>, Jiayi Luo<sup>2,6</sup>, Tianyu He, Xin Jin<sup>2,4</sup>,  
Zhibo Chen<sup>1,2\*</sup>

<sup>1</sup>School of Information Science and Technology, University of Science and Technology of  
China, Hefei, China.

<sup>2</sup>Zhongguancun Academy, Beijing, China.

<sup>3</sup>the State Key Laboratory of Multimodal Artificial Intelligence Systems, Institute of  
Automation, Chinese Academy of Sciences, Beijing, China.

<sup>4</sup>Eastern Institute of Technology, Ningbo, China.

<sup>5</sup>College of Information Science and Electronic Engineering, Zhejiang University,  
Hangzhou, China.

<sup>6</sup>School of Computer Science and Engineering, Beihang University, Beijing, China.

\*Corresponding author(s). E-mail(s): [chenzhibo@ustc.edu.cn](mailto:chenzhibo@ustc.edu.cn);

Contributing authors: [hanxinzhu@mail.ustc.edu.cn](mailto:hanxinzhu@mail.ustc.edu.cn); [deeptimhe@gmail.com](mailto:deeptimhe@gmail.com);

## Abstract

Recent developments in generative models and large-scale datasets have substantially advanced 3D world generation, facilitating a broad range of domains including spatial intelligence, embodied intelligence, and autonomous driving. While achieving remarkable progress, existing approaches to 3D world generation typically prioritize appearance prediction with limited modeling of the underlying geometry, leading to issues such as unreliable scene structure estimation and degraded cross-view consistency. To address these limitations, motivated by the coarse-to-fine nature of human visual perception, we propose **GTA**, a novel image-to-3D world generation method following a **Geometry-Then-Appearance** paradigm. Specifically, given a single input image, to improve the structural fidelity of synthesized 3D scenes, GTA adopts a two-stage framework with two dedicated video diffusion models, which first generate coarse geometric structure from novel viewpoints and then synthesize fine-grained appearance conditioned on the predicted geometry. To further enhance cross-view appearance consistency, we introduce a random latent shuffle strategy during the training process, along with a test-time scaling scheme that improves perceptual quality without compromising quantitative performance. Extensive experiments have demonstrated that our proposed method consistently outperforms existing approaches in terms of fidelity, visual quality, and geometric accuracy. Moreover, GTA is shown to be effective as a general enhancement module that further improves the generation quality of existing image-to-3D world pipelines, as well as supporting multiple downstream applications and exhibiting favorable data efficiency during model training, highlighting its versatility and broad applicability. Project page: <https://hanxinzhu-lab.github.io/GTA/>.

**Keywords:** 3D Generation, World Generation, Generative Model, Video Diffusion Model

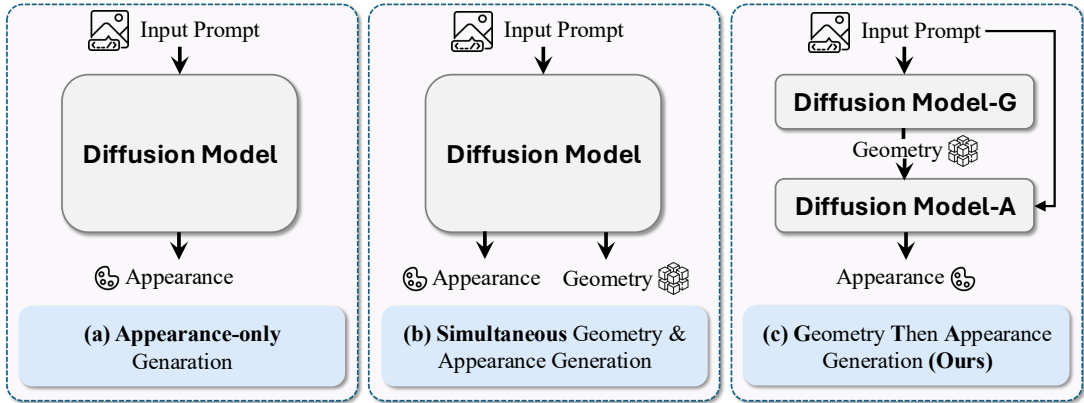


**Fig. 1 Comparisons of pipelines for 3D world generation.** (a) Appearance-only generation, which focuses on synthesizing appearance without modeling scene geometry. (b) Simultaneous geometry and appearance generation, which jointly predicts both modalities within a single diffusion model. (c) **Geometry-Then-Appearance generation (ours)**, which first estimates multi-view geometric structure and subsequently synthesizes appearance conditioned on the predicted geometry.

## 1 Introduction

As the fundamental medium for human perception, understanding, and action, 3D spatial environments underpin all activities in the physical world. For decades, the digital representation, reconstruction, and generation of such complex environments have remained a central and long-standing challenge in computer vision, computer graphics, and artificial intelligence [1–6]. As one of the key research directions, 3D generation [2, 5, 7–10] focuses on synthesizing 3D assets with faithful spatial structure and appearance from multimodal inputs such as text and images. By bridging the physical and digital worlds, it serves as a foundation for a broad spectrum of domains, ranging from embodied intelligence [11, 12] to world modeling [13–15].

Early approaches to 3D generation primarily focused on object-level synthesis [16–19], where individual 3D objects or simple scenes were generated by distilling priors from pretrained generative models. While effective for isolated objects, such object-centric formulations are inherently limited in scalability and struggle to capture the complex spatial layouts and long-range relationships present in real-world scenes. Recently, driven by the powerful spatiotemporal modeling capabilities of video generative models [20–22], together with the availability of large-scale internet data [23, 24], research has increasingly shifted towards scene-level 3D generation [25–27], aiming to synthesize

complex 3D worlds with coherent geometry and consistent appearance across different viewpoints.

Despite achieving encouraging progress, as shown in Fig. 1(a), most existing scene-level approaches remain largely appearance-centric [28–31], exhibiting a pronounced bias towards texture synthesis with limited modeling of the underlying geometry. However, since geometric structure provides the fundamental spatial scaffold that constrains scene layout and enforces cross-view consistency, insufficient geometric modeling leaves appearance synthesis inherently underconstrained, typically resulting in unreliable scene structure estimation and view-inconsistent renderings. These observations suggest that, for 3D world generation, the construction of geometry and appearance is equally essential, and both should be carefully considered to achieve a faithful and consistent 3D scene.

To this end, a straightforward way is to simultaneously predict geometry and appearance within a unified framework [32, 33], aiming to obtain a coherent scene representation, as shown in Fig. 1(b). However, simultaneous prediction is inherently challenging [34], as geometry and appearance differ substantially in learning difficulty, data distributions, and uncertainty. As a result, optimizing both modalities at the same time often induces mutual interference, leading to geometric distortions, appearance flickering, and degraded cross-view consistency.

In nature, human visual perception has been extensively characterized as exhibiting a coarse-to-fine organization [35, 36], wherein global scene structure is processed prior to fine-scale surface details. Inspired by this perceptual principle, we posit that 3D world generation should similarly prioritize the establishment of geometric structure before appearance modeling, thereby reducing ambiguity and alleviating the interference arising from simultaneous prediction.

Guided by this perspective, in this paper we propose **GTA**, a novel image-to-3D world generation framework that follows a **Geometry-Then-Appearance** paradigm. Specifically, GTA casts 3D world generation as a hierarchical modeling process that explicitly disentangles geometric structure from appearance synthesis. As demonstrated in Fig. 1(c), leveraging two dedicated video diffusion models (referred to as Diffusion Model-G and Diffusion Model-A), the framework first constructs a coarse yet globally consistent geometric representation of the scene across novel viewpoints. This geometry-aware representation then serves as an explicit structural prior to guide a subsequent appearance synthesis stage, enabling fine-grained texture generation under well-defined spatial constraints and resulting in structurally faithful 3D scenes.

However, video diffusion models are typically pretrained to capture temporal dynamics in natural videos [37], thereby encoding strong inductive biases towards motion continuity and temporal ordering. When directly transferred to cross-view 3D world generation, these biases become misaligned with the inherently spatial and order-invariant nature of multi-view observations. Hence, under large viewpoint disparities between the input and target views, the appearance diffusion model is prone to texture drifting, which degrades overall synthesis quality. To address this challenge, we introduce a simple yet effective random latent shuffle strategy during the training process. By weakening the model’s dependence on view-order-specific cues, this strategy encourages the learning of spatially consistent appearance patterns under varying viewpoints, leading to more robust appearance synthesis and improved cross-view consistency in the generated 3D scenes.

Despite the aforementioned improvements, synthesizing novel views under large disparities remains a challenging problem. In such cases,

the limited spatial coverage of the input image provides weak constraints for distant target viewpoints, causing direct single-pass synthesis to yield implausible geometry. To address this limitation, we propose a test-time scaling strategy that progressively refines the generated scene by incorporating reliable views from earlier synthesis rounds as additional conditioning. Combined with a masked-warping mechanism, this strategy substantially enhances perceptual plausibility without compromising quantitative performance.

Beyond its core design, we further demonstrate experimentally that GTA exhibits strong extensibility and practical versatility. In particular, GTA can be seamlessly integrated as a post-hoc enhancement module to improve the performance of a wide range of existing image-to-3D pipelines, highlighting its compatibility with diverse generation paradigms. Moreover, the proposed framework readily generalizes to related tasks such as 3D scene editing and video depth estimation, underscoring its applicability beyond 3D scene synthesis. Notably, GTA also demonstrates favorable data efficiency, achieving competitive performance with substantially reduced training data, which further enhances its practicality in real-world scenarios.

The main contributions of this paper are summarized as follows:

- We propose GTA, a novel image-to-3D world generation framework that adopts a two-stage geometry-then-appearance paradigm, in which geometric structure is first estimated and subsequently used to guide appearance synthesis. To the best of our knowledge, GTA represents the first attempt to explicitly decouple geometry and appearance in a stage-wise manner for scene-level image-to-3D generation.
- We introduce a simple yet effective random latent shuffle strategy for training video diffusion models in cross-view 3D world generation, which promotes the learning of spatially consistent appearance representations and significantly improves cross-view coherence under large viewpoint variations.
- We propose a test-time scaling strategy to further improve the quality of generated 3D worlds. By progressively refining the synthesized scene using reliable views from earlier generations, together with a masked-warping mechanism,

this strategy substantially improves perceptual plausibility while maintaining comparable quantitative performance.

- Extensive experimental results demonstrate that GTA achieves state-of-the-art performance in 3D world generation, as well as exhibiting strong versatility as a general enhancement module and supporting multiple downstream applications with favorable data efficiency during model training.

## 2 Related Works

### 2.1 Video Generation

Recently, significant progress has been made in video generation [37–39], driven by the rapid development of large-scale datasets and generative models. By extending image generation models to the temporal domain, these approaches explicitly model spatiotemporal dependencies and enable the synthesis of high-quality video sequences with improved visual fidelity and temporal coherence [21, 40–46].

Building upon this foundation, a growing body of research has extended video generative models to a variety of downstream scenarios, including controllable video generation [47–50], long-range video modeling [51–54], and efficient video synthesis [55, 56]. For example, VideoControlNet [57] augments video diffusion models with an explicit control pathway that conditions generation on structural cues, enabling precise spatiotemporal control without retraining the backbone model. MoC [58] addresses the challenge of extended temporal generation by dynamically combining multiple contextual windows at different temporal scales, allowing the model to capture both short-term dynamics and long-range dependencies for coherent long-video synthesis. To further improve efficiency, BSA [55] proposes a sparsity-aware attention mechanism that restricts spatiotemporal interactions to structured bidirectional neighborhoods, significantly accelerating video diffusion training while maintaining generation quality.

In light of the remarkable progress of video generative models in modeling complex spatiotemporal dynamics, we observe that multi-view observations of a static 3D scene can be naturally formulated as a structured video sequence indexed

by camera viewpoints rather than time. This perspective motivates us to adopt video generative models as a principled foundation for 3D world generation in this work.

### 2.2 3D Generation

3D generation has recently attracted increasing attention due to its broad applicability in areas such as autonomous driving, robotics, and immersive environments [2, 5, 7–10]. To this end, existing approaches can be broadly categorized into two paradigms: 3D object generation, which concentrates on synthesizing individual objects [16–19], and 3D world generation, which targets the generation of complex scenes with multiple objects and rich structural layouts [25–27]. We review these two lines of work below.

#### *3D object generation.*

Owing to the absence of large-scale datasets with precise 3D annotations, early approaches to 3D object generation primarily relied on pre-trained 2D generative priors and optimization-based frameworks without explicit 3D supervision [16, 17, 59–61]. For example, NeuralLift-360 [60] optimizes a NeRF representation guided by CLIP, enforcing semantic consistency between novel-view renderings and the reference image in a shared feature space, thereby enabling approximate 360° radiance field reconstruction from a single input image. Make-It-3D [61] further incorporates pre-trained diffusion models into the optimization process, leveraging their strong generative priors to impose perceptual and semantic constraints on novel-view renderings, which leads to higher-quality 3D asset generation. Despite their strong visual performance, these approaches fundamentally rely on scene-specific optimization and are highly sensitive to the quality of pre-trained 2D priors, resulting in substantial computational overhead and limited scalability, which hampers their practical applicability.

Recently, with the emergence of large-scale 3D datasets providing explicit geometric and appearance supervision (e.g., Objaverse [62], which offers diverse object shapes and textures at scale) research has gradually shifted toward training feed-forward 3D generation models in an end-to-end manner [63–67]. Leveraging explicit 3D supervision, these approaches avoid per-scene

optimization and significantly improve efficiency and scalability. For instance, Zero123 [64] introduces a latent diffusion-based framework for view-conditioned 3D generation, enabling the synthesis of novel views given a reference image and target camera poses. Building upon this paradigm, One-2-3-45 [65] and its enhanced variant One-2-3-45++ [66] lift the multi-view images generated by Zero123 into 3D space by enforcing multi-view consistency, reconstructing complete textured 3D meshes with substantially reduced inference time. In a similar spirit, Wonder3D [67] proposes a cross-domain diffusion framework that jointly models 2D appearance and 3D geometry, enabling single-image 3D generation by aligning diffusion processes across image and 3D domains.

However, these methods are largely object-centric, typically assuming a single foreground object in a simplified environment, and thus are not well suited for modeling complex 3D scenes with multiple objects and rich structural layouts.

### 3D world generation.

In contrast to object-centric settings, 3D world generation aims to synthesize large-scale environments with complex geometry, diverse appearances, and long-range consistency, which poses significantly greater challenges [68–71]. Early approaches such as [68] and [69] address this problem by progressively extending views along predefined camera trajectories, leveraging pre-trained image inpainting models to hallucinate unseen regions while preserving global scene continuity. Building upon this incremental generation paradigm, subsequent methods such as [70] and [69] improve generation efficiency by accelerating the scene expansion process, enabling faster construction of coherent large-scale 3D worlds.

Recently, several works have begun to incorporate view-controllable video diffusion models to enhance scene-level modeling [28, 30, 72–74]. For instance, CamCtrl3D [73] conditions an image-to-video diffusion model on predefined 3D camera trajectories by explicitly encoding camera parameters into the latent diffusion process, enabling precise camera control and allowing users to freely navigate virtual 3D scenes from a single input image. Similarly, ViewCrafter [28] adopts video diffusion models as strong generative priors, where coarse scene geometry is first estimated using

methods such as DUST3R [75], and then leveraged to condition video generation for completing unobserved regions. This design enables the synthesis of high-fidelity novel-view sequences with large viewpoint variations from one or a few input images. Building upon this line of research, methods such as FlexWorld [72] and Gen3C [74] further introduce persistent 3D cache representations. By iteratively accumulating and reusing intermediate 3D representations, these approaches can gradually construct complete scenes that support 360° exploration under single-image conditions.

However, while these methods have achieved impressive results, they are typically appearance-centric or rely on simultaneous geometry and appearance generation, where structural information and visual content are either implicitly entangled or jointly optimized. In contrast, in this paper we propose GTA, a novel 3D generation framework that follows a geometry-then-appearance paradigm, explicitly separating geometric modeling from appearance synthesis to reduce cross-modal interference and improve both geometric reliability and appearance consistency.

## 3 Preliminaries

### 3.1 Video Diffusion Models

Diffusion models [76, 77] have recently emerged as a powerful class of generative models for high-dimensional data synthesis, including images and videos. A diffusion model consists of a *forward diffusion process*  $q$  that gradually corrupts clean data with Gaussian noise, and a *reverse denoising process*  $p_\theta$  that learns to invert this corruption process and recover the data distribution.

Given a clean video sample  $\mathbf{x}_0 \sim q_0(\mathbf{x}_0)$ , the forward process incrementally adds noise over  $\mathcal{T}$  timesteps according to

$$\mathbf{x}_t = \alpha_t \mathbf{x}_0 + \sigma_t \boldsymbol{\epsilon}, \quad \boldsymbol{\epsilon} \sim \mathcal{N}(\mathbf{0}, \mathbf{I}), \quad (1)$$

where  $\alpha_t$  and  $\sigma_t$  are predefined noise schedules. The reverse process parameterized by  $\theta$  aims to denoise  $\mathbf{x}_t$  by predicting the injected noise  $\boldsymbol{\epsilon}$  using a neural network  $\boldsymbol{\epsilon}_\theta$ , which is trained by minimizing the standard noise prediction objective:

$$\min_{\theta} \mathbb{E}_{t \sim \mathcal{U}(0, \mathcal{T}), \boldsymbol{\epsilon} \sim \mathcal{N}(\mathbf{0}, \mathbf{I})} \left[ \|\boldsymbol{\epsilon}_\theta(\mathbf{x}_t, t) - \boldsymbol{\epsilon}\|_2^2 \right]. \quad (2)$$

To improve computational efficiency for high-resolution video generation, latent diffusion models (LDMs) are widely adopted [78]. Instead of performing diffusion directly in pixel space, video frames are first encoded into a compact latent representation using a pretrained variational autoencoder (VAE). Both the forward noising process and the reverse denoising process are then carried out in this latent space, significantly reducing computational cost and memory consumption. The final video is obtained by decoding the denoised latent sequence back to the pixel space through the VAE decoder.

By explicitly modeling temporal correlations across frames, video diffusion models capture rich spatiotemporal dynamics and generate temporally coherent video sequences. In this work, we build upon an image-to-video diffusion framework, which aligns naturally with our goal of synthesizing novel views from a single-view input by interpreting multi-view observations as structured video sequences.

## 4 Methods

Given an input image, our goal is to synthesize a consistent 3D world that captures the complexity of real-world scenes. To this end, existing methods typically either emphasize appearance generation without explicitly modeling the underlying geometry [28, 72, 74, 79], or jointly predict geometry and appearance within a single framework [32–34]. While achieving promising results, the lack of explicit geometric constraints or the tight coupling between geometry and appearance, which are two modalities with distinct learning characteristics, often leads to ambiguities during generation, resulting in unreliable structure estimation and degraded cross-view consistency.

To solve this problem, we propose **GTA**, a novel method that formulates image-to-3D world generation in a stage-wise manner, explicitly disentangling geometry generation from appearance synthesis (Sec. 4.1). To further enhance cross-view appearance consistency, we introduce a random latent shuffle strategy during training (Sec. 4.2), together with a test-time scaling strategy that improves scene synthesis quality during inference (Sec. 4.3). Details are provided below.

### 4.1 Geometry Then Appearance Video Diffusion

Motivated by the coarse-to-fine nature of human visual perception [35, 36], where global scene structure is inferred prior to fine-grained surface details, we posit that scene-level 3D generation should likewise prioritize geometric structure before appearance synthesis. In this context, geometry provides a global and view-consistent spatial scaffold, while appearance encodes higher-frequency visual details that are naturally conditioned on such structure.

Building upon this insight, we design GTA to explicitly follow a hierarchical modeling principle. Specifically, GTA decomposes image-to-3D world generation into two successive stages, each handled by a dedicated video diffusion model. In the first stage, a geometry video diffusion model predicts a multi-view geometric representation of the scene from the input image. In the second stage, an appearance video diffusion model synthesizes fine-grained textures conditioned on the predicted geometry, enabling appearance generation to be guided by explicit structural priors rather than inferred implicitly.

Formally, let  $I_0 \in \mathbb{R}^{H \times W \times 3}$  denote the input image captured from a reference viewpoint  $v_0$ . Our goal is to generate a set of view-consistent observations  $\mathcal{O}$  of the 3D world from a collection of  $T$  target viewpoints  $\{v_t\}_{t=1}^T$ . Each observation consists of a geometric component and a corresponding appearance component, which we denote as

$$\mathcal{O} = \{(G_t, A_t)\}_{t=1}^T, \quad (3)$$

where  $G_t$  represents the geometric structure of the scene observed from viewpoint  $v_t$ , and  $A_t$  denotes the corresponding RGB appearance. Details of the geometry and appearance modeling are illustrated below.

#### *Geometry Video Diffusion.*

As shown in Fig. 2, for the input image  $I_0$ , we first estimate its depth map  $D_0 \in \mathbb{R}^{H \times W \times 1}$  using a pretrained monocular depth estimator. This estimated depth provides an explicit geometric proxy of the scene, allowing us to reason about cross-view spatial correspondence in a principled manner. Leveraging this geometric prior, we construct coarse multi-view observations via depth-based

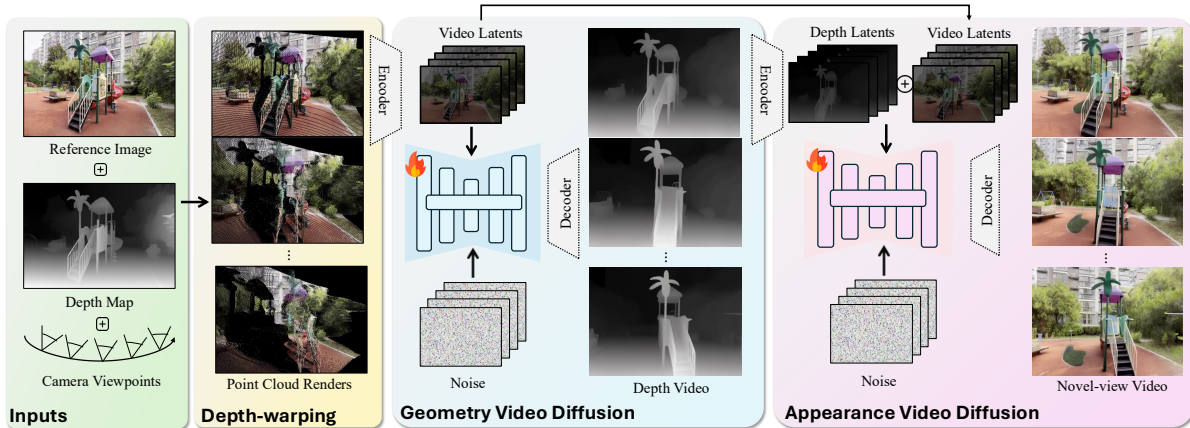


**Fig. 2 Pipeline of our proposed geometry then appearance video diffusion.** Starting from a single input image, the method first performs geometry video diffusion to generate a view-consistent multi-view video depth via depth-based warping. Conditioned on the predicted geometry, an appearance video diffusion model then synthesizes a coherent novel-view RGB video with fine-grained textures.

warping, serving as structured conditioning for subsequent geometry modeling.

Specifically, the depth map  $D_0$  is first lifted into a set of 3D point clouds  $\mathcal{P}$  using the following equation:

$$\mathcal{P} = \{\mathbf{P}_i \in \mathbb{R}^3 \mid \mathbf{P}_i = D_0(\mathbf{u}_i) \mathbf{K}^{-1} \tilde{\mathbf{u}}_i\}, \quad (4)$$

where  $i \in \{1, \dots, HW\}$  indexes pixel locations in the reference image,  $\mathbf{u}_i \in \mathbb{R}^2$  denotes the corresponding image coordinate,  $\tilde{\mathbf{u}}_i$  is its homogeneous representation, and  $\mathbf{K}$  is the camera intrinsic matrix. The resulting point set  $\mathcal{P}$  is then rendered into each target viewpoint  $v_t$ , producing a set of warped RGB observations  $\{\hat{I}_t\}_{t=1}^T$ . Owing to occlusions and the limited spatial coverage of the reference view, these warped observations are inherently partial, forming an incomplete multi-view sequence.

Subsequently, we adopt a video diffusion model to infer a geometrically consistent scene representation from these warped multi-view inputs. Considering that depth provides a compact yet expressive proxy for geometric structure, we represent scene geometry using depth maps and formulate geometry modeling as the synthesis of a complete depth video conditioned on the warped observations.

To this end, the warped RGB sequence  $\{\hat{I}_t\}_{t=1}^T$  is first encoded by a video variational autoencoder (VAE) to obtain a sequence of geometry-aware

video latents  $\mathbf{z}^{\text{rgb}}$ . In parallel, the reference-view depth map  $D_0$  is encoded by the same VAE to produce a depth latent  $\mathbf{z}^{D_0}$  corresponding to the input view. These two latent representations are then concatenated along the channel dimension and fed into the geometry video diffusion model, which performs denoising in the latent space to generate a complete depth video. Finally, the predicted latent sequence is decoded by the VAE decoder to obtain the refined multi-view depth maps. Formally, the whole process can be represented as

$$\begin{aligned} \{G_t\}_{t=1}^T &= \mathcal{D}(\Phi_g(\mathbf{z}^{\text{rgb}} \oplus \mathbf{z}^{D_0})), \\ \mathbf{z}^{\text{rgb}} &= \mathcal{E}(\{\hat{I}_t\}_{t=1}^T), \quad \mathbf{z}^{D_0} = \mathcal{E}(D_0), \end{aligned} \quad (5)$$

where  $\mathcal{E}(\cdot)$  and  $\mathcal{D}(\cdot)$  denote the encoder and decoder of a shared video VAE, respectively,  $\Phi_g(\cdot)$  denotes the geometry video diffusion model operating in the latent space,  $\oplus$  represents channel-wise concatenation.

### *Appearance Video Diffusion.*

In the second stage, given the generated multi-view depth video  $\{G_t\}_{t=1}^T$ , our goal is to synthesize a view-consistent appearance video  $\{A_t\}_{t=1}^T$  that faithfully captures the surface textures and visual details. Compared to geometry generation, appearance synthesis involves higher-frequency information and is inherently more ambiguous, especially under large viewpoint changes. We

therefore condition appearance modeling explicitly on the predicted geometry, allowing appearance generation to be guided by reliable structural cues.

Specifically, the generated multi-view depth video  $\{G_t\}_{t=1}^T$  is first encoded by the same video VAE to obtain a sequence of geometry latents  $\mathbf{z}^{\text{geo}}$ . The geometry latents are then concatenated with the partial RGB latents  $\mathbf{z}^{\text{rgb}}$  obtained in the previous stage along the channel dimension, and passed through a lightweight projection module to match the input dimensionality required by the diffusion backbone. To further strengthen geometric conditioning and encourage structure-aligned appearance synthesis, the projected latent is fused with the geometry latent via a residual addition before being fed into the appearance video diffusion model. This design biases the diffusion process toward generating textures that are consistent with the underlying geometric structure, while preserving sufficient flexibility for modeling high-frequency appearance details. The whole process is denoted as follows:

$$\begin{aligned} \{A_t\}_{t=1}^T &= \mathcal{D}(\Phi_a(\mathbf{h}^a)), \\ \mathbf{h}^a &= \Pi(\mathbf{z}^{\text{rgb}} + \mathbf{z}^{\text{geo}}) + \mathbf{z}^{\text{geo}}, \\ \mathbf{z}^{\text{geo}} &= \mathcal{E}(\{G_t\}_{t=1}^T), \end{aligned} \quad (6)$$

where  $\Pi(\cdot)$  denotes the lightweight projection module,  $\Phi_a(\cdot)$  denotes the appearance video diffusion model.

## 4.2 Random Latent Shuffle

After defining the architecture of our geometry then appearance video diffusion models, we now consider how to effectively train it for 3D world synthesis. Intuitively, one may directly adopt the standard training protocol of video diffusion models, treating multi-view observations as ordered video sequences and optimizing the model to predict denoised target views. However, we find that such a straightforward adaptation often leads to noticeable cross-view inconsistencies in practice. For example, regions that are black in the input view may gradually fade into gray as the diffusion process synthesizes a novel target view, particularly under large viewpoint disparities between the input and target views, as shown in Fig. 8(a).

We attribute this behavior primarily to the inductive biases inherited from video diffusion pretraining. Specifically, video diffusion models are typically optimized to model temporal dynamics in natural videos, where appearance evolution is strongly coupled with smooth motion and a well-defined temporal order. As a result, the learned representations implicitly favor continuity along the sequence dimension and encourage gradual appearance transitions between adjacent frames.

When such models are directly applied to cross-view 3D world synthesis, these temporal assumptions become suboptimal. Multi-view observations of a static scene are inherently spatial in nature and invariant to view ordering, yet the model continues to interpret view indices as a proxy for temporal progression. This misalignment becomes particularly problematic under large viewpoint changes, where enforcing temporal smoothness across views introduces spurious appearance correlations. Consequently, the diffusion process may gradually alter texture statistics across views, leading to visible drifting artifacts and degraded cross-view consistency in the synthesized results.

To solve this problem, we propose a simple yet effective training strategy, termed *Random Latent Shuffle*. The core idea of this strategy is to attenuate the model’s dependence on view-order-specific correlations, while largely preserving the strong generative priors acquired through video diffusion pretraining. Concretely, as shown in Fig. 3, during training, we stochastically permute the ordering of latent representations associated with different target views with a predefined probability before they are processed by the video diffusion model, which is formulated as:

$$\tilde{\mathbf{z}} = \boldsymbol{\pi}(\mathbf{z}), \boldsymbol{\pi} \sim \begin{cases} \mathcal{U}(\mathcal{S}_T), & \text{with probability } p, \\ \text{Id}, & \text{with probability } 1 - p, \end{cases} \quad (7)$$

where  $\mathbf{z}$  denotes the latent representations, and  $\tilde{\mathbf{z}}$  is the corresponding latent after random shuffling. The operator  $\boldsymbol{\pi}$  represents a permutation applied along the view dimension. With probability  $p$ ,  $\boldsymbol{\pi}$  is sampled uniformly from the permutation group  $\mathcal{S}_T$ , denoted by  $\mathcal{U}(\mathcal{S}_T)$ , which randomly reorders the  $T$  target views; otherwise, the identity permutation  $\text{Id}$  is applied, leaving the latent ordering

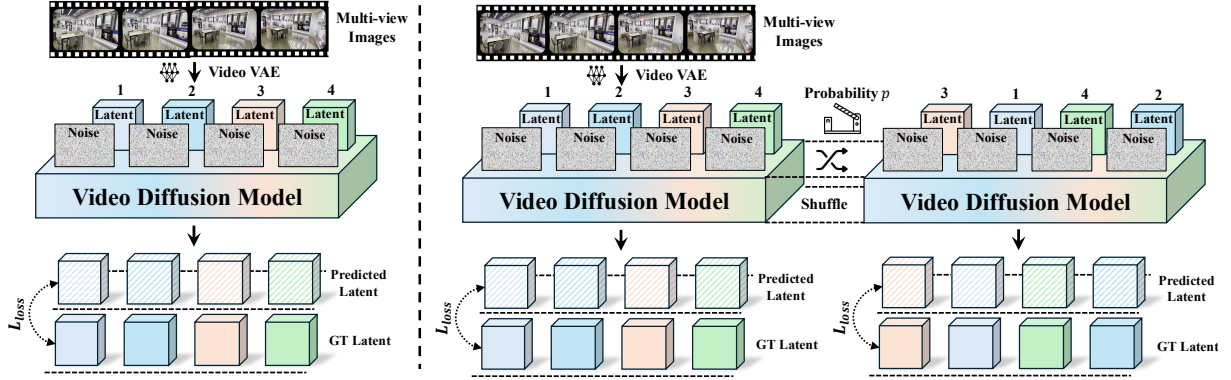


**Fig. 3 Pipeline of our proposed random latent shuffle strategy.** During training, the latent representations corresponding to different target views are randomly permuted with probability  $p$  before being fed into the video diffusion model. The same permutation is applied to both predicted and ground-truth latents, preserving supervision while discouraging view-order-dependent correlations. This strategy encourages the model to treat multi-view observations as unordered spatial samples rather than temporally ordered frames, and is only applied during training.

unchanged. The probability  $p$  controls the frequency of applying random latent shuffle during training.

During training, the same permutation  $\pi$  is applied to both the latent to be denoised and the corresponding ground-truth latent, ensuring that their correspondence is preserved after shuffling. The video diffusion model is then optimized using the standard noise prediction objective, following the conventional training protocol. In this way, random latent shuffle perturbs the view ordering without altering the underlying supervision signal, effectively discouraging the model from exploiting spurious order-dependent correlations.

Notably, the random latent shuffle is only employed as a training-time regularization strategy. At inference time, no shuffling is applied, and the latent representations are fed into the video diffusion model in the target view order.

### 4.3 Test-time Scaling

Although the proposed random latent shuffle strategy substantially enhances cross-view consistency, synthesizing high-fidelity novel views under large viewpoint disparities remains challenging at inference time. In such cases, the limited spatial coverage provided by the input observation imposes weak geometric and appearance constraints on distant target views, often leading to implausible structures or visually inconsistent results.

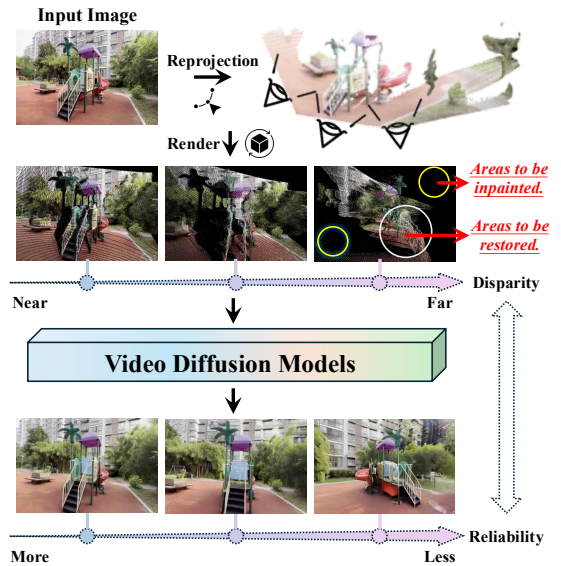


**Fig. 4 Two key observations from single-pass inference.** The reliability of synthesized views decreases as the viewpoint disparity from the input increases. Meanwhile, the rendered partial observations contain two distinct region types: visible regions requiring appearance restoration, and unobserved regions that must be hallucinated via inpainting.

To address this limitation, we pursue a test-time scaling strategy that enhances synthesis quality by more effectively leveraging the model’s intrinsic generative capacity and test-time information, without incurring additional training

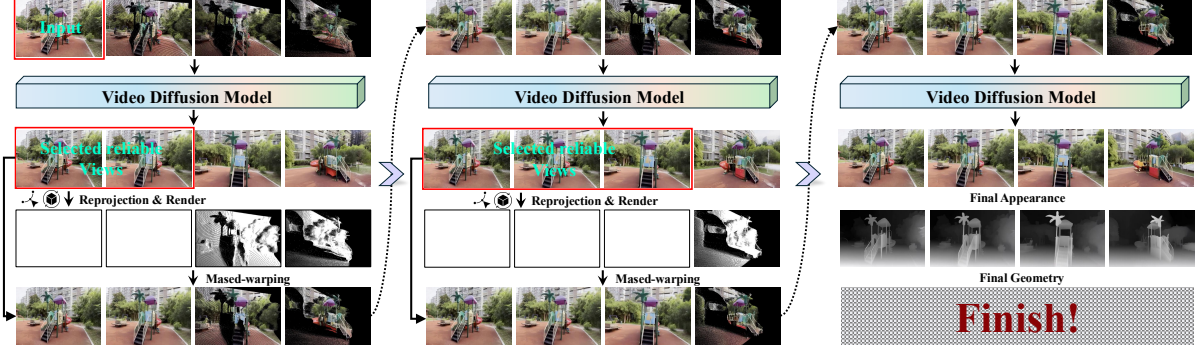


**Fig. 5 Pipeline of the proposed test-time scaling strategy.** Starting from an initial inference pass, a subset of reliable views is progressively selected and reprojected to construct updated partial observations. Through masked-warping, restored regions are fixed while unreliable regions are suppressed, and the video diffusion model is iteratively conditioned on the refined inputs, enabling coarse-to-fine synthesis of distant target views with improved stability and cross-view consistency.

overhead. To this end, as shown in Fig. 4, we begin by making two key observations from a single-pass inference setting.

First, the reliability of synthesized novel views exhibits a strong dependence on their distance to the input view. *Views with relatively small disparities tend to be generated more faithfully*, as abundant geometric and appearance cues can be effectively transferred from the input image. In contrast, views that lie farther are constrained by substantially weaker visual evidence and are therefore more susceptible to structural inaccuracies and visual artifacts, making their rendering inherently less reliable.

Second, in our pipeline, where a partial RGB video sequence is rendered from point-based representations and subsequently completed by video diffusion models to synthesize a full multi-view RGB sequence, *the models are actually required to handle two fundamentally different types of generation simultaneously*. On the one hand, for regions that are visible from the input view under the target viewpoints, the rendered sequence provides partial but imperfect information, typically affected by distortions or rendering artifacts. These regions mainly demand appearance correction and refinement rather than content hallucination, and are therefore referred to as *areas to be restored*. On the other hand, for regions that are not visible from the input views under the target viewpoints, no reliable visual evidence is available, and the models must rely on their learned generative priors to plausibly synthesize the missing content. We refer to these regions as *areas to be inpainted*.

---

### Algorithm 1 Test-time Scaling

---

- 1: **Input:** input image  $I$ , target viewpoints  $\{v_t\}_{t=1}^T$ , trained video diffusion models
  - 2: **Output:** synthesized RGB sequence  $\{A_t\}_{t=1}^T$
  - 3: Perform an initial inference pass using Eq. 5 and Eq. 6 to obtain  $\{A_t\}_{t=1}^T$
  - 4: Initialize the reliable view set  $\mathcal{R} \leftarrow \{1, \dots, Q\}$
  - 5: **while**  $\mathcal{R}$  does not cover all target views **do**
  - 6:     Perform depth-based warping using Eq. 4 with  $I$  and  $\{A_t\}_{t \in \mathcal{R}}$
  - 7:     Derive a binary visibility mask sequence  $\{\hat{M}_t\}_{t=1}^T$
  - 8:     Apply masked-warping to obtain a masked partial RGB sequence  $\{\hat{I}_t\}_{t=1}^T$
  - 9:     Update  $\{A_t\}_{t=1}^T$  via video diffusion conditioned on  $\{\hat{I}_t\}_{t=1}^T$
  - 10:    Expand  $\mathcal{R}$  to include additional  $Q$  target views
  - 11: **end while**
  - 12: **return**  $\{A_t\}_{t=1}^T$
- 

Based on the above two observations, as illustrated in Fig. 5 and Alg. 1, our test-time scaling proceeds as follows. Without loss of generality, we assume that the target views are ordered by increasing viewpoint distance from the input view. After an initial inference pass with Eq. 5 and Eq. 6, the first  $Q$  views in the generated RGB sequence  $\{A_t\}_{t=1}^T$  are regarded as reliable. Together with the input view, they are then used to perform depth-based warping using Eq. 4 along the same  $T$  target viewpoints  $\{v_t\}_{t=1}^T$ , yielding an updated partial observations.

From these warped results, we further derive a binary mask sequence  $\{\hat{M}_t\}_{t=1}^T$  that indicates pixel-wise visibility, where  $M_t(\mathbf{x}) = 1$  denotes pixels that can be rendered from the available views, and  $\hat{M}_t(\mathbf{x}) = 0$  corresponds to regions that remain unobserved. Following the second observation, regions corresponding to *areas to be restored* are expected to be largely reliable at this stage, as coarse but informative cues can already be inferred from the input view and are reasonably approximated after an initial forward pass of the model. We therefore apply the mask sequence to the synthesized RGB outputs  $\{A_t\}_{t=1}^T$ , retaining the restored regions while suppressing unreliable content in the *areas to be inpainted*, thereby producing a masked partial RGB sequence  $\{\hat{I}_t\}_{t=1}^T$ . We refer to this operation as masked-warping. By fixing restored regions, the models are freed from jointly performing restoration and hallucination, effectively reducing interference between the two fundamentally different modes and yielding more stable synthesis under large disparities.

The resulting masked partial RGB sequence is then fed back into the video diffusion models as input for the next inference round. This procedure is performed iteratively in a progressive manner, where an increasing set of synthesized views is treated as reliable at each iteration. At every stage, the currently reliable views are used to perform depth-based warping and masked-warping to construct an updated partial RGB sequence, which serves as conditioning for subsequent inference. The process continues until all target views are incorporated or a predefined number of iterations is reached.

In essence, this test-time scaling strategy facilitates a coarse-to-fine inference paradigm, where reliable visual evidence is progressively accumulated and leveraged to guide subsequent synthesis. As a result, distant target views benefit from increasingly stronger conditioning, leading to more stable and visually consistent novel view generation under large disparities, while incurring no additional training overhead.

## 5 Experiments

### 5.1 Experimental Setups

**Datasets.** We conduct training on the DL3DV dataset [80], which comprises approximately 10K

real-world scenes captured from diverse camera viewpoints. For each scene, we curate 10 high-quality video sequences featuring varying camera trajectories, resulting in a total of 100K training samples.

At inference time, we evaluate our model on two datasets. The first is the official DL3DV evaluation split [80], which contains 55 scenes that are strictly disjoint from the training set. For this split, we construct 55 videos, each composed of a sequence of multi-view images. Given the first frame of each video as input, the model is required to generate the remaining frames. In addition, we assess the generalization ability of our method on a fully held-out dataset, RealEstate10K [81]. We randomly sample 100 scenes from the dataset and remove those containing insufficient multi-view images, resulting in 79 valid scenes. Following the same protocol as DL3DV, we construct 79 multi-view videos and perform inference on this set.

**Baseline and Metrics.** We compare our method with several representative state-of-the-art approaches spanning two fundamental paradigms of 3D scene generation. Specifically, we compare against two categories of approaches: (i) *appearance-only generation* methods that focus solely on synthesizing visual appearance (e.g., texture and color) without explicitly modeling scene geometry, and (ii) methods that *simultaneously generate appearance and geometry* by jointly reasoning about visual content and structural information. For the former, we compare with See3D [79], ViewCrafter [28], FlexWorld [72], Gen3C [74], and TrajectoryCrafter [82], covering both U-Net-based methods (See3D and ViewCrafter) and Diffusion Transformer (DiT)-based methods (FlexWorld, Gen3C, and TrajectoryCrafter); for the latter, we include Voyager [32] as a representative baseline.

We evaluate the performance of all methods from three complementary perspectives. First, to assess *fidelity*, we adopt widely used pixel- and perceptual-level metrics, including PSNR, SSIM, and LPIPS, which respectively measure reconstruction accuracy, structural similarity, and perceptual distance. Second, to evaluate overall *visual quality*, we employ FID and Q-Align [83]. FID measures the distribution-level consistency

Metrics	See3D	ViewCrater	TrajectoryCrafter	FlexWorld	Gen3C	Voyager	Ours
<b>DL3DV Dataset</b>							
PSNR $\uparrow$	15.86	15.09	15.82	15.39	16.15	15.23	<b>17.47</b>
SSIM $\uparrow$	0.483	0.409	0.454	0.428	0.473	0.406	<b>0.525</b>
LPIPS $\downarrow$	0.425	0.457	0.412	0.402	0.433	0.436	<b>0.342</b>
FID $\downarrow$	65.70	61.15	43.94	39.53	43.56	60.90	<b>38.32</b>
Q-Align-V (quality) $\uparrow$	3.045	3.066	3.361	3.312	2.954	3.305	<b>3.385</b>
Q-Align-V (aesthetics) $\uparrow$	2.258	2.224	2.392	2.280	2.097	2.292	<b>2.421</b>
Q-Align-I (quality) $\uparrow$	2.887	2.787	3.088	3.060	2.813	3.209	<b>3.215</b>
Q-Align-I (aesthetics) $\uparrow$	1.962	1.927	2.023	1.901	1.817	2.041	<b>2.082</b>
T-err $\downarrow$	0.003	0.008	0.005	<b>0.001</b>	0.003	0.008	<b>0.001</b>
R-err $\downarrow$	0.017	0.029	0.026	0.019	0.022	0.025	<b>0.013</b>
<b>RealEstate Dataset</b>							
PSNR $\uparrow$	15.97	13.52	16.08	15.77	16.46	15.80	<b>17.01</b>
SSIM $\uparrow$	0.595	0.472	0.589	0.597	0.612	0.574	<b>0.644</b>
LPIPS $\downarrow$	0.380	0.485	0.376	0.380	0.368	0.398	<b>0.341</b>
FID $\downarrow$	44.99	50.37	32.36	27.48	31.08	37.08	<b>26.72</b>
Q-Align-V (quality) $\uparrow$	2.877	2.608	3.237	3.198	2.889	3.260	<b>3.455</b>
Q-Align-V (aesthetics) $\uparrow$	1.980	1.796	2.236	2.127	1.968	2.229	<b>2.417</b>
Q-Align-I (quality) $\uparrow$	2.623	2.474	3.198	2.956	2.731	3.063	<b>3.287</b>
Q-Align-I (aesthetics) $\uparrow$	1.609	1.535	1.946	1.751	1.665	1.898	<b>2.002</b>
T-err $\downarrow$	0.038	0.103	0.032	<b>0.024</b>	0.034	0.035	0.026
R-err $\downarrow$	0.065	0.129	0.080	0.060	0.075	0.094	<b>0.041</b>

**Table 1 Quantitative comparison across fidelity, perceptual quality, and geometric accuracy on the DL3DV and RealEstate datasets.**  $\uparrow$  and  $\downarrow$  indicate that higher and lower values correspond to better performance, respectively. Best, second-best, and third-best results are highlighted in red, orange, and yellow. Our method consistently achieves superior performance on both datasets. Notably, all results here are reported using single-pass inference without test-time scaling, and the effect of test-time scaling is analyzed separately in the ablation study.

between generated and real videos, while Q-Align provides fine-grained, human-aligned quality assessment across multiple perceptual dimensions. Specifically, Q-Align evaluates both video-level and frame-level perceptual quality and aesthetics, including Q-Align-V (quality), Q-Align-V (aesthetics), Q-Align-I (quality), and Q-Align-I (aesthetics). All Q-Align scores are normalized to a range of  $[0, 5]$ , where higher values indicate better alignment with human visual perception. Finally, following the evaluation protocol of CameraCtrl [30], we assess *geometric accuracy* by estimating camera poses from the generated videos and measuring their deviation from the ground-truth camera trajectories. We report rotation error (R-err), which reflects discrepancies between rotation matrices, and translation error (T-err), which measures differences in camera translation vectors.

**Implementation Details.** Our model is obtained via supervised fine-tuning (SFT) based

on CogVideo-X-5B [84], and generates videos consisting of 49 frames at a spatial resolution of  $720 \times 480$ . During training, camera poses are estimated using VGGT [85], while per-frame depth maps are obtained using Video Depth Anything [86]. At inference time, depth estimation for the input image is performed using Depth Anything V2 [87]. For the random latent shuffle strategy, we set the shuffle probability  $p$  to 0.5. For the test-time scaling, the reliable view window size  $Q$  is set to 5. All training experiments are conducted on 8 NVIDIA A800 GPUs, where the appearance video diffusion and geometry video diffusion models are each trained for 40,000 iterations. During inference, all experiments are performed on a single NVIDIA A800 GPU, with peak GPU memory consumption of approximately 20 GB.

## 5.2 Main Results

Tab. 1 reports the quantitative comparison on the DL3DV and RealEstate datasets. Overall, our



**Fig. 6 Qualitative comparison between our method and state-of-the-art approaches.** Our method generates visually coherent scenes with improved detail preservation and geometric consistency, as highlighted in yellow circles.

method consistently outperforms all competing approaches across fidelity, perceptual quality, and geometric accuracy on both datasets, demonstrating its effectiveness and robustness across different generation paradigms and evaluation settings.

On the DL3DV dataset, our method achieves the best performance on all fidelity metrics, obtaining the highest PSNR and SSIM as well as the lowest LPIPS, indicating superior reconstruction accuracy and perceptual similarity. In terms

of visual quality, our method also yields the lowest FID and consistently achieves the highest scores across all Q-Align dimensions, including both video-level and frame-level quality and aesthetics, suggesting improved alignment with human visual perception. Furthermore, our method demonstrates strong geometric consistency. We achieve the lowest rotation error (R-err) and jointly lowest translation error (T-err), highlighting more accurate camera trajectory estimation and improved geometric alignment with the ground-truth scene structure.

On the RealEstate dataset, which is fully held out from training for our method but used during training by other methods, our approach still maintains clear advantages. Specifically, we obtain the best results on PSNR, SSIM, LPIPS, and FID, and consistently outperform all counterparts across all Q-Align metrics. In addition, our method achieves the lowest R-err and competitive T-err, further validating its strong generalization capability.

In addition to quantitative evaluation, we further provide qualitative comparisons in Fig. 6 to visually assess the perceptual differences among methods. For See3D, the generated results tend to exhibit noticeable loss of fine-grained details, where high-frequency textures are over-smoothed, leading to blurred appearances in fine structures and reduced visual sharpness. For other appearance-only methods, such as ViewCrafter, FlexWorld, Gen3C, and TrajectoryCrafter, synthesis under large viewpoint changes is often accompanied by geometric distortions and texture inconsistency, manifested as deformed object structures, spatial misalignment of structural elements, and view-dependent texture variations, ultimately leading to reduced geometric coherence and visual consistency. For voyager, the synthesized results often suffer from excessive color saturation and unnatural color shifts, along with noticeable discrepancies in fine-grained details relative to the input image. In contrast, our proposed method effectively preserves fine-grained visual details and enforces consistent geometry and texture appearance, resulting in 3D scenes that remain visually coherent and faithful to the input image under large viewpoint changes.

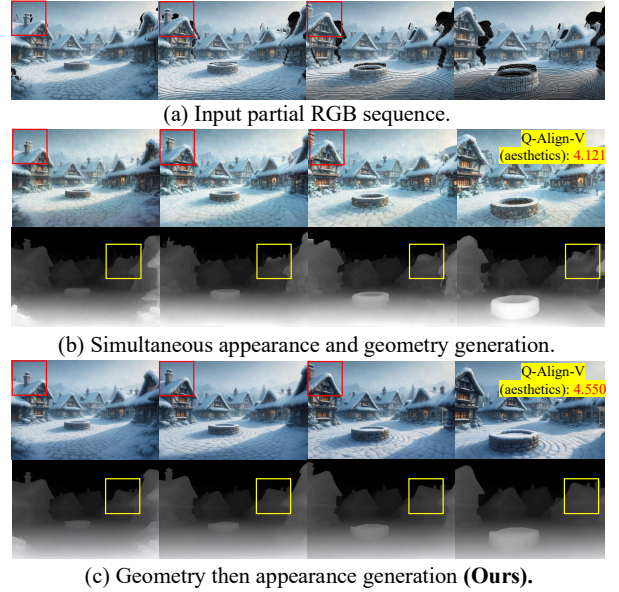


**Fig. 7 Qualitative ablation study on geometry-then-appearance generation (GTA).** Compared to simultaneous appearance-and-geometry generation, GTA produces more consistent textures and stable geometry. The red and yellow boxes highlight representative regions where the contrast between the two approaches is particularly evident.

### 5.3 Ablation Studies

To demonstrate the effectiveness of our proposed designs, we conduct ablation studies on geometry then appearance generation, random latent shuffle and test-time scaling.

#### *Geometry Then Appearance Generation.*

To evaluate the effectiveness of the proposed geometry-then-appearance generation strategy, we randomly select 20 DL3DV scenes with large camera viewpoint changes and conduct an ablation comparison against Voyager, which adopts a simultaneous geometry-and-appearance prediction paradigm.

As demonstrated in Fig. 7 and Tab. 2, simultaneous prediction is intrinsically challenging, as geometry and appearance exhibit substantially different learning characteristics in terms of optimization difficulty, data distributions, and uncertainty levels. When optimized jointly, these heterogeneous modalities tend to interfere with each other, causing unstable learning dynamics. In

Generation Strategy	PSNR $\uparrow$	SSIM $\uparrow$	LPIPS $\downarrow$
SAG	15.03	0.391	0.471
GTA (Ours)	<b>17.14</b>	<b>0.502</b>	<b>0.367</b>

**Table 2 Quantitative ablation study on generation strategies using scenes with large viewpoint changes.** SAG denotes simultaneous appearance and geometry generation, while GTA denotes geometry-then-appearance generation. GTA consistently improves reconstruction fidelity compared to SAG.

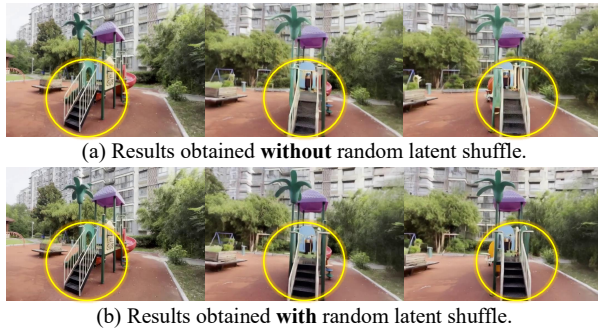


**Fig. 8 Qualitative ablation study on random latent shuffle.** Without random latent shuffle, the generated appearance tends to drift across viewpoints, leading to inconsistent textures, as highlighted by the yellow circles. Random latent shuffle mitigates such view-dependent appearance drifting and improves cross-view consistency.

practice, this interference not only leads to inconsistent appearance synthesis, such as texture flickering and color instability, but also degrades geometric estimation, resulting in temporally unstable depth predictions with noticeable flickering and structural distortions across frames.

In contrast, our geometry-then-appearance strategy decouples geometric reasoning from appearance synthesis, allowing the model to first converge to a stable and coherent geometric representation. This geometry-aware foundation subsequently provides reliable structural guidance for appearance generation, effectively mitigating cross-modal interference and yielding more consistent depth estimation, more stable geometry, and improved appearance coherence.

### *Random Latent Shuffle.*

We further investigate the effect of the proposed random latent shuffle strategy. During training of the video diffusion model, random latent shuffle is applied by randomly permuting the input

Training Setting	PSNR $\uparrow$	SSIM $\uparrow$	LPIPS $\downarrow$
<b>Without</b> Random Latent Shuffle	16.83	0.497	0.389
<b>With</b> Random Latent Shuffle	<b>17.47</b>	<b>0.525</b>	<b>0.342</b>

**Table 3 Quantitative ablation study on random latent shuffle.** Introducing random latent shuffle during training improves reconstruction fidelity and perceptual quality by alleviating view-order-dependent appearance drifting.

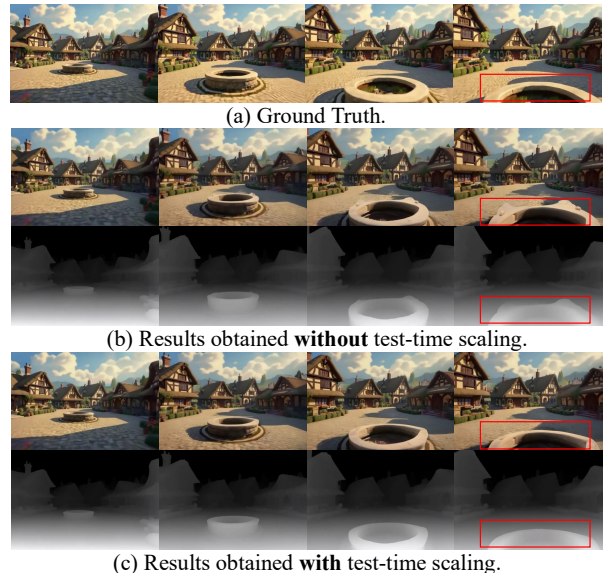


**Fig. 9 Qualitative ablation study on test time scaling.** Test-time scaling improves geometric plausibility and visual consistency under large viewpoint changes compared to single-pass inference.

latent features with a predefined probability. This strategy weakens the model’s reliance on view-order-specific correlations inherited from video diffusion pretraining, thereby discouraging spurious cross-view dependencies and improving consistency under large viewpoint changes.

As demonstrated in Fig. 8 and Tab. 3, without random latent shuffle, the synthesized scenes exhibit noticeable appearance drifting as the viewpoint changes. For example, regions that are black in the input image progressively fade into gray in the generated results.

In contrast, introducing random latent shuffle during training acts as an effective regularization, resulting in more stable texture statistics and improved cross-view appearance consistency.

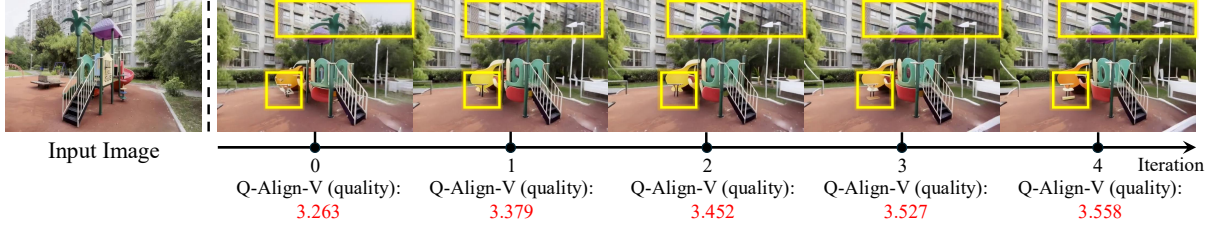


**Fig. 10 Visualization of intermediate results of test-time scaling.** As the number of scaling iterations increases, the synthesized results become perceptually more plausible and geometrically more reasonable, while quantitative metrics improve progressively, indicating a stable and effective refinement process.

Test-time Scaling	Without	With
PSNR $\uparrow$	<b>17.47</b>	17.35
SSIM $\uparrow$	0.525	<b>0.531</b>
LPIPS $\downarrow$	0.342	<b>0.340</b>
FID $\downarrow$	38.32	<b>34.54</b>
Q-Align-V (quality) $\uparrow$	3.385	<b>3.603</b>
Q-Align-V (aesthetics) $\uparrow$	2.421	<b>2.564</b>
Q-Align-I (quality) $\uparrow$	3.215	<b>3.488</b>
Q-Align-I (aesthetics) $\uparrow$	2.082	<b>2.224</b>
T-err $\downarrow$	0.001	<b>0.001</b>
R-err $\downarrow$	0.013	<b>0.011</b>

**Table 4 Quantitative ablation study on test-time scaling.** The proposed strategy consistently improves reconstruction fidelity, perceptual quality, and geometric accuracy.

### Test-time scaling.

We further study the effect of the proposed test-time scaling strategy, which aims to improve synthesis quality under large viewpoint changes without introducing additional training cost. Although the random latent shuffle strategy significantly enhances cross-view consistency during training, generating high-fidelity novel views at inference time remains challenging when target viewpoints are far from the input view. In such cases, the limited visual evidence provided by the input image yields weak geometric and appearance constraints, often resulting in implausible structures or visually inconsistent results.

The key intuition behind test-time scaling is that the reliability of synthesized views is not uniform: views closer to the input observation tend to be more accurate, while distant views are more prone to artifacts. Based on this observation, we progressively expand the set of reliable views at inference time and reuse them as additional conditioning signals for subsequent synthesis.

As demonstrated in Fig. 9, without test-time scaling, the synthesized results often exhibit implausible geometric estimations in regions corresponding to viewpoints far from the input view. In particular, distant views are prone to structural distortions and unstable depth predictions, reflecting insufficient geometric constraints during single-pass inference. In contrast, with test-time scaling enabled, the model produces more geometrically plausible and visually consistent results by progressively incorporating reliable synthesized views as additional conditioning, thereby stabilizing geometry and improving appearance coherence under large viewpoint changes. As shown in Tab. 4, test-time scaling consistently improves performance across multiple metrics, with particularly pronounced gains on all Q-Align scores at both the video and frame levels. These results suggest that the proposed strategy effectively enhances the perceptual plausibility of the synthesized content and achieves closer alignment with human visual perception under large viewpoint changes.

Moreover, as illustrated in Fig. 10, we further visualize the intermediate results at each iteration of test-time scaling. As the number of scaling iterations increases, the synthesized novel views exhibit progressively improved geometric plausibility and visual consistency, demonstrating that the proposed strategy enables a stable and monotonic refinement process.

## 5.4 Post-doc Enhancement

Beyond serving as a standalone 3D-aware generation framework, our method can also be seamlessly integrated as a post-processing enhancement module for existing image-to-3D scene generation pipelines. Specifically, given cross-view RGB



**Fig. 11 Qualitative results of post-hoc enhancement.** Applying our method as a post-processing module corrects implausible structures and suppresses view-dependent artifacts in the original outputs, resulting in more geometrically plausible and visually coherent generations.

video sequences produced by prior methods, our approach can directly take these outputs as inputs and further refine them through the proposed geometry video diffusion and appearance video diffusion models.

As demonstrated in Tab. 5 and Fig. 11, our method consistently improves the quality of results produced by different image-to-3D scene generation pipelines when applied as a post-hoc enhancement module. From a quantitative perspective, integrating our approach leads to consistent gains in PSNR and SSIM, along

Method	PSNR $\uparrow$	SSIM $\uparrow$	LPIPS $\downarrow$
FlexWorld	15.39	0.428	0.402
FlexWorld + Ours	<b>16.62</b>	<b>0.488</b>	<b>0.358</b>
Gen3C	16.15	0.473	0.433
Gen3C + Ours	<b>16.83</b>	<b>0.501</b>	<b>0.364</b>
Voyager	15.23	0.406	0.436
Voyager + Ours	<b>16.98</b>	<b>0.508</b>	<b>0.361</b>

**Table 5 Post-hoc enhancement results on different image-to-3D scene generation methods.**

Applying our method as a post-processing module consistently improves reconstruction fidelity and perceptual quality across evaluated baselines.

with noticeable reductions in LPIPS, indicating improved reconstruction fidelity and perceptual similarity. From a qualitative perspective, our method effectively corrects implausible structures and suppresses view-dependent artifacts present in the original outputs. As shown in Fig. 11, the enhanced results exhibit more coherent geometry, clearer fine-grained details, and improved cross-view appearance consistency, resulting in visually more plausible and sharper scene generations.

Notably, these improvements are achieved without retraining or modifying the original pipelines, highlighting the flexibility and general applicability of our method as a plug-and-play post-processing enhancement.

## 5.5 Applications on Downstream Tasks

Benefiting from the geometry-then-appearance generation paradigm, our method naturally extends to multiple downstream tasks, such as 3D scene editing and video depth estimation. Details are provided below.

### 3D scene editing.

To achieve 3D scene editing, we first employ a pretrained image editing model to modify the reference view (i.e., the first frame) of the input scene, while retaining the video depth estimated from the original scene as a representation of the underlying geometry. The edited reference image is subsequently rendered along the original camera trajectories using the preserved depth information to construct a partial RGB sequence. This

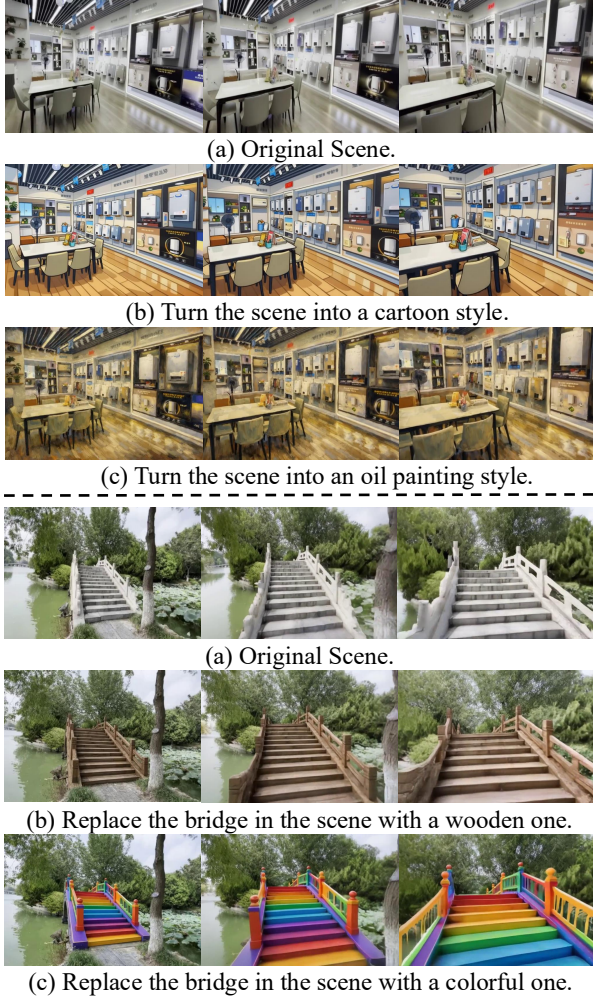


**Fig. 12 Qualitative results of 3D scene editing.** Our method supports both global appearance stylization (e.g., transforming a scene into cartoon or oil painting styles) and local object-level editing (e.g., replacing a stone bridge with a wooden or colored one), while preserving geometric coherence and cross-view consistency.

partial sequence, together with the corresponding depth video, is then provided as conditioning input to our appearance video diffusion model, which synthesizes the edited scene across all target viewpoints. Through this process, the edited appearance is consistently propagated to novel views while preserving geometric coherence.

As demonstrated in Fig. 12, our approach supports both global and local 3D scene editing in a unified manner. For global editing, the method enables scene-level style transfer, such as transforming an input scene into a cartoon or oil

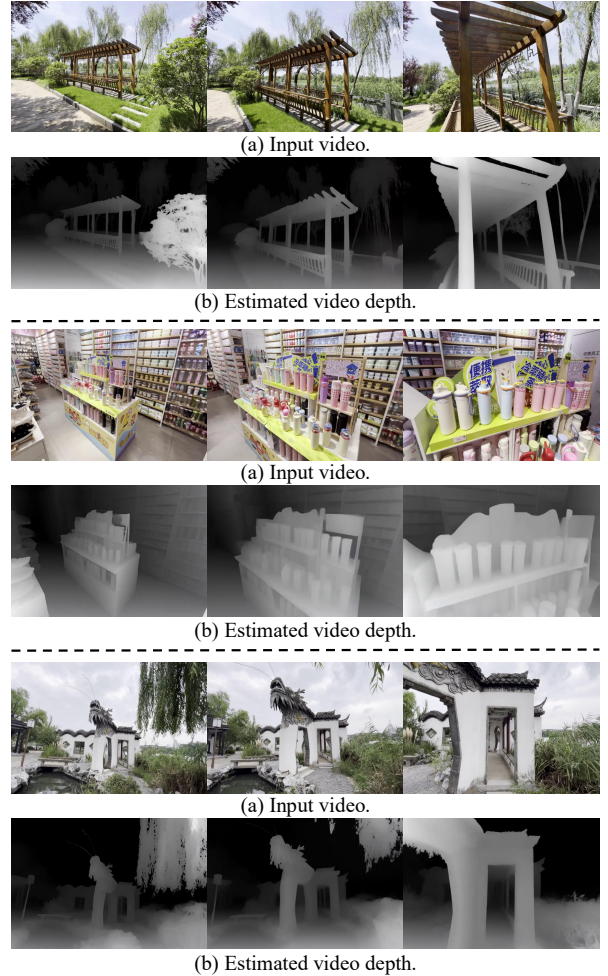


**Fig. 13 Qualitative results of video depth estimation.** Our geometry video diffusion model produces temporally consistent depth maps that capture fine-grained structural details across frames.

painting style. For local editing, our framework allows targeted modifications of specific scene elements, such as replacing a stone bridge with a wooden or colored bridge, without affecting the surrounding structures. These results illustrate the flexibility of our method in handling diverse editing requirements.

#### *Video depth estimation.*

Our method also naturally supports video depth estimation by leveraging the proposed geometry video diffusion model. Given an RGB video as input, the geometry video diffusion model can

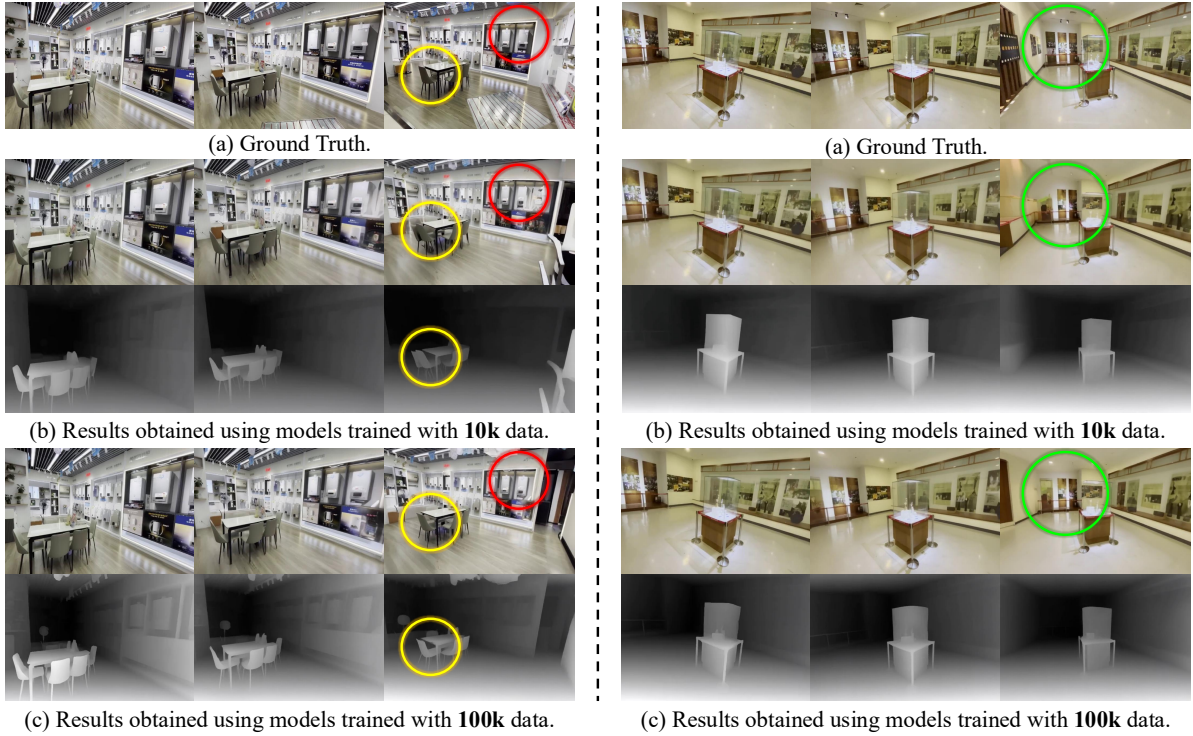


**Fig. 14 Qualitative results under different training data scales.** Even with only 10K training samples, our method recovers the overall scene structure with reasonable geometric accuracy, while increasing the data scale progressively improves fine-grained details and texture fidelity.

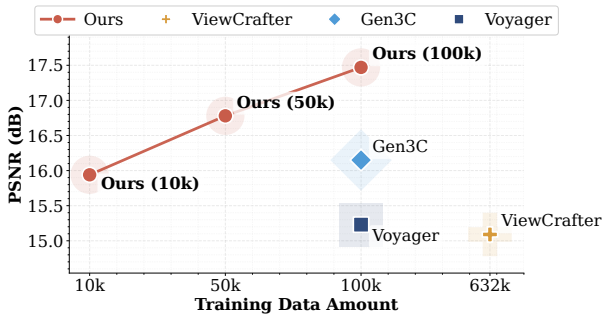


**Fig. 15 Data efficiency comparison.** Our method achieves comparable or even better performance than state-of-the-art approaches with an order of magnitude fewer training samples, and continues to improve steadily as the training data scale increases.

be directly applied to infer a temporally consistent depth sequence without requiring additional supervision or task-specific training. As illustrated in Fig. 13, the estimated depth maps exhibit strong temporal consistency across frames and capture fine-grained structural details of the scene,

demonstrating the effectiveness of our approach for video-level depth estimation.

## 5.6 Data Efficiency

Our proposed method also demonstrates strong data efficiency, enabling reliable geometry generation and appearance synthesis even with limited training data. As illustrated in Fig. 15, our approach achieves performance comparable to, or even exceeding, state-of-the-art methods while using an order of magnitude fewer training samples. Moreover, as the training data scale increases, our method continues to exhibit steady performance improvements, indicating favorable scalability. As shown in Fig. 14, even when trained with only 10K samples, our model is able to recover the overall scene structure with reasonable geometric accuracy and visual coherence. As the training data scale increases, the generated results exhibit progressively enhanced fine-grained details and improved texture fidelity, indicating

stronger appearance modeling while maintaining stable geometry.

This strong data efficiency can be attributed to the proposed geometry-then-appearance modeling strategy. By prioritizing geometric structure learning, the model first acquires low-frequency, highly regular scene representations that can be reliably learned from limited data, thereby reducing the complexity of the learning task. Subsequently, appearance synthesis is guided by these stable structural priors that reduce ambiguity and narrow the hypothesis space, thus enabling high-quality texture generation with limited data. Together, this formulation leads to a substantially more data-efficient training process.

## 6 Conclusion

In this paper, we propose GTA, a novel image-to-3D world generation framework that follows a geometry-then-appearance paradigm. By aligning the generation process with the coarse-to-fine characteristics of human visual perception, GTA adopts a two-stage video diffusion architecture that first establishes structurally coherent 3D geometry and then synthesizes high-quality, view-consistent appearance conditioned on the predicted geometry. To further enhance cross-view consistency, we introduce a random latent shuffle strategy that effectively mitigates view-order-dependent appearance drift during training. In addition, we present a test-time scaling strategy that progressively refines the generated scenes at inference time, improving perceptual quality without introducing additional training overhead. Extensive experiments demonstrate that GTA consistently outperforms existing state-of-the-art methods in terms of structural fidelity, visual realism, and geometric accuracy across multiple benchmarks. Beyond standalone performance, GTA can be naturally incorporated as a post-hoc enhancement module into existing image-to-3D generation pipelines, delivering consistent improvements without architectural modifications. Moreover, the proposed framework generalizes effectively to a range of downstream tasks, including 3D scene editing and video depth estimation. Finally, GTA exhibits strong data efficiency, achieving competitive performance under reduced training data regimes, highlighting its

practicality and scalability for real-world 3D generation applications.

**Data Availability Statements.** The DL3DV dataset [80] is available at <https://github.com/DL3DV-10K/Dataset>. The RealEstate10K [81] dataset is available at <https://google.github.io/realestate10k/>. The code of this paper will be available upon publication.

**Conflict of interest.** The authors have no relevant financial or non-financial interests to disclose.

## References

- [1] Butime, J., Gutierrez, I., Corzo, L.G., Espronceda, C.F.: 3d reconstruction methods, a survey. In: Proceedings of the First International Conference on Computer Vision Theory and Applications, pp. 457–463 (2006)
- [2] Li, X., Zhang, Q., Kang, D., Cheng, W., Gao, Y., Zhang, J., Liang, Z., Liao, J., Cao, Y.-P., Shan, Y.: Advances in 3d generation: A survey. arXiv preprint arXiv:2401.17807 (2024)
- [3] Peng, S., Genova, K., Jiang, C., Tagliasacchi, A., Pollefeys, M., Funkhouser, T., *et al.*: Openscene: 3d scene understanding with open vocabularies. In: Proceedings of the IEEE/CVF Conference on Computer Vision and Pattern Recognition, pp. 815–824 (2023)
- [4] Samavati, T., Soryani, M.: Deep learning-based 3d reconstruction: a survey. *Artificial Intelligence Review* **56**(9), 9175–9219 (2023)
- [5] Wen, B., Xie, H., Chen, Z., Hong, F., Liu, Z.: 3d scene generation: A survey. arXiv preprint arXiv:2505.05474 (2025)
- [6] Zia, M.Z., Stark, M., Schindler, K.: Towards scene understanding with detailed 3d object representations. *International Journal of Computer Vision* **112**(2), 188–203 (2015)
- [7] Li, M., Zhou, P., Liu, J.-W., Keppo, J., Lin, M., Yan, S., Xu, X.: Instant3d: Instant text-to-3d generation. *International Journal of Computer Vision* **132**(10), 4456–4472 (2024)

- [8] Moschoglou, S., Ploumpis, S., Nicolaou, M.A., Papaioannou, A., Zafeiriou, S.: 3dfacegan: Adversarial nets for 3d face representation, generation, and translation. *International Journal of Computer Vision* **128**(10), 2534–2551 (2020)
- [9] Di, D., Yang, J., Luo, C., Xue, Z., Chen, W., Yang, X., Gao, Y.: Hyper-3dg: Text-to-3d gaussian generation via hypergraph. *International Journal of Computer Vision* **133**(5), 2886–2909 (2025)
- [10] Song, W., Zhang, X., Guo, Y., Li, S., Hao, A., Qin, H.: Automatic generation of 3d scene animation based on dynamic knowledge graphs and contextual encoding. *International Journal of Computer Vision* **131**(11), 2816–2844 (2023)
- [11] Yang, Y., Sun, F.-Y., Weihs, L., VanderBilt, E., Herrasti, A., Han, W., Wu, J., Haber, N., Krishna, R., Liu, L., *et al.*: Holodeck: Language guided generation of 3d embodied ai environments. In: *Proceedings of the IEEE/CVF Conference on Computer Vision and Pattern Recognition*, pp. 16227–16237 (2024)
- [12] Wang, X., Liu, L., Cao, Y., Wu, R., Qin, W., Wang, D., Sui, W., Su, Z.: Embodiedgen: Towards a generative 3d world engine for embodied intelligence. *arXiv preprint arXiv:2506.10600* (2025)
- [13] Kong, L., Yang, W., Mei, J., Liu, Y., Liang, A., Zhu, D., Lu, D., Yin, W., Hu, X., Jia, M., *et al.*: 3d and 4d world modeling: A survey. *arXiv preprint arXiv:2509.07996* (2025)
- [14] Ding, J., Zhang, Y., Shang, Y., Zhang, Y., Zong, Z., Feng, J., Yuan, Y., Su, H., Li, N., Sukiennik, N., *et al.*: Understanding world or predicting future? a comprehensive survey of world models. *ACM Computing Surveys* **58**(3), 1–38 (2025)
- [15] Zheng, W., Chen, W., Huang, Y., Zhang, B., Duan, Y., Lu, J.: Occworld: Learning a 3d occupancy world model for autonomous driving. In: *European Conference on Computer Vision*, pp. 55–72 (2024). Springer
- [16] Poole, B., Jain, A., Barron, J.T., Mildenhall, B.: Dreamfusion: Text-to-3d using 2d diffusion. *arXiv preprint arXiv:2209.14988* (2022)
- [17] Lin, C.-H., Gao, J., Tang, L., Takikawa, T., Zeng, X., Huang, X., Kreis, K., Fidler, S., Liu, M.-Y., Lin, T.-Y.: Magic3d: High-resolution text-to-3d content creation. In: *Proceedings of the IEEE/CVF Conference on Computer Vision and Pattern Recognition*, pp. 300–309 (2023)
- [18] Raj, A., Kaza, S., Poole, B., Niemeyer, M., Ruiz, N., Mildenhall, B., Zada, S., Aberman, K., Rubinstein, M., Barron, J., *et al.*: Dreambooth3d: Subject-driven text-to-3d generation. In: *Proceedings of the IEEE/CVF International Conference on Computer Vision*, pp. 2349–2359 (2023)
- [19] Wang, H., Du, X., Li, J., Yeh, R.A., Shakhnarovich, G.: Score jacobian chaining: Lifting pretrained 2d diffusion models for 3d generation. In: *Proceedings of the IEEE/CVF Conference on Computer Vision and Pattern Recognition*, pp. 12619–12629 (2023)
- [20] Hong, W., Ding, M., Zheng, W., Liu, X., Tang, J.: Cogvideo: Large-scale pretraining for text-to-video generation via transformers. *arXiv preprint arXiv:2205.15868* (2022)
- [21] Gupta, A., Yu, L., Sohn, K., Gu, X., Hahn, M., Li, F.-F., Essa, I., Jiang, L., Lezama, J.: Photorealistic video generation with diffusion models. In: *European Conference on Computer Vision*, pp. 393–411 (2024). Springer
- [22] Bar-Tal, O., Chefer, H., Tov, O., Herrmann, C., Paiss, R., Zada, S., Ephrat, A., Hur, J., Liu, G., Raj, A., *et al.*: Lumiere: A space-time diffusion model for video generation. In: *SIGGRAPH Asia 2024 Conference Papers*, pp. 1–11 (2024)
- [23] Nan, K., Xie, R., Zhou, P., Fan, T., Yang, Z., Chen, Z., Li, X., Yang, J., Tai, Y.: Openvid-1m: A large-scale high-quality dataset for text-to-video generation. *arXiv preprint arXiv:2407.02371* (2024)

- [24] Wang, Y., He, Y., Li, Y., Li, K., Yu, J., Ma, X., Li, X., Chen, G., Chen, X., Wang, Y., et al.: Internvid: A large-scale video-text dataset for multimodal understanding and generation. arXiv preprint arXiv:2307.06942 (2023)
- [25] Sun, W., Chen, S., Liu, F., Chen, Z., Duan, Y., Zhang, J., Wang, Y.: Dimensionx: Create any 3d and 4d scenes from a single image with controllable video diffusion. arXiv preprint arXiv:2411.04928 (2024)
- [26] Bahmani, S., Skorokhodov, I., Qian, G., Siarohin, A., Menapace, W., Tagliasacchi, A., Lindell, D.B., Tulyakov, S.: Ac3d: Analyzing and improving 3d camera control in video diffusion transformers. In: Proceedings of the Computer Vision and Pattern Recognition Conference, pp. 22875–22889 (2025)
- [27] Liang, H., Cao, J., Goel, V., Qian, G., Korolev, S., Terzopoulos, D., Plataniotis, K.N., Tulyakov, S., Ren, J.: Wonderland: Navigating 3d scenes from a single image. In: Proceedings of the Computer Vision and Pattern Recognition Conference, pp. 798–810 (2025)
- [28] Yu, W., Xing, J., Yuan, L., Hu, W., Li, X., Huang, Z., Gao, X., Wong, T.-T., Shan, Y., Tian, Y.: Viewcrafter: Taming video diffusion models for high-fidelity novel view synthesis. arXiv preprint arXiv:2409.02048 (2024)
- [29] Zhang, S., Xu, H., Guo, S., Xie, Z., Bao, H., Xu, W., Zou, C.: Spatialcrafter: Unleashing the imagination of video diffusion models for scene reconstruction from limited observations. In: Proceedings of the IEEE/CVF International Conference on Computer Vision, pp. 27794–27805 (2025)
- [30] He, H., Xu, Y., Guo, Y., Wetzstein, G., Dai, B., Li, H., Yang, C.: Cameractrl: Enabling camera control for text-to-video generation. arXiv preprint arXiv:2404.02101 (2024)
- [31] Wang, Z., Yuan, Z., Wang, X., Li, Y., Chen, T., Xia, M., Luo, P., Shan, Y.: Motionctrl: A unified and flexible motion controller for video generation. In: ACM SIGGRAPH 2024 Conference Papers, pp. 1–11 (2024)
- [32] Huang, T., Zheng, W., Wang, T., Liu, Y., Wang, Z., Wu, J., Jiang, J., Li, H., Lau, R., Zuo, W., et al.: Voyager: Long-range and world-consistent video diffusion for explorable 3d scene generation. ACM Transactions on Graphics (TOG) **44**(6), 1–15 (2025)
- [33] Dai, Y., Jiang, F., Wang, C., Xu, M., Qi, Y.: Fantasyworld: Geometry-consistent world modeling via unified video and 3d prediction. arXiv preprint arXiv:2509.21657 (2025)
- [34] Zhang, H., Chen, K., Zhang, Z., Chen, H.H., Lyu, Y., Zhang, Y., Yang, S., Zhou, K., Chen, Y.: Dualcamctrl: Dual-branch diffusion model for geometry-aware camera-controlled video generation. arXiv preprint arXiv:2511.23127 (2025)
- [35] Navon, D.: Forest before trees: The precedence of global features in visual perception. Cognitive psychology **9**(3), 353–383 (1977)
- [36] Watt, R.: Scanning from coarse to fine spatial scales in the human visual system after the onset of a stimulus. Journal of the Optical Society of America A **4**(10), 2006–2021 (1987)
- [37] Xing, Z., Feng, Q., Chen, H., Dai, Q., Hu, H., Xu, H., Wu, Z., Jiang, Y.-G.: A survey on video diffusion models. ACM Computing Surveys **57**(2), 1–42 (2024)
- [38] Waseem, F., Shahzad, M.: Video is worth a thousand images: Exploring the latest trends in long video generation. ACM Computing Surveys **58**(6), 1–35 (2025)
- [39] Ma, W., Yang, X., Jiao, L., Li, L., Liu, X., Liu, F., Chen, P., Yang, Y., Ma, M., Sun, L., et al.: Video diffusion generation: comprehensive review and open problems. Artificial Intelligence Review **58**(11), 338 (2025)
- [40] Tulyakov, S., Liu, M.-Y., Yang, X., Kautz, J.: Mocogan: Decomposing motion and content for video generation. In: Proceedings of the IEEE Conference on Computer Vision and

Pattern Recognition, pp. 1526–1535 (2018)

- [41] Li, Y., Min, M., Shen, D., Carlson, D., Carin, L.: Video generation from text. In: Proceedings of the AAAI Conference on Artificial Intelligence, vol. 32 (2018)
- [42] Singer, U., Polyak, A., Hayes, T., Yin, X., An, J., Zhang, S., Hu, Q., Yang, H., Ashual, O., Gafni, O., et al.: Make-a-video: Text-to-video generation without text-video data. arXiv preprint arXiv:2209.14792 (2022)
- [43] Tian, Y., Yang, L., Yang, H., Gao, Y., Deng, Y., Chen, J., Wang, X., Yu, Z., Tao, X., Wan, P., et al.: Videotetris: Towards compositional text-to-video generation. *Advances in Neural Information Processing Systems* **37**, 29489–29513 (2024)
- [44] Chen, S., Xu, M., Ren, J., Cong, Y., He, S., Xie, Y., Sinha, A., Luo, P., Xiang, T., Perez-Rua, J.-M.: Gentrion: Diffusion transformers for image and video generation. In: Proceedings of the IEEE/CVF Conference on Computer Vision and Pattern Recognition, pp. 6441–6451 (2024)
- [45] Wang, Y., Chen, X., Ma, X., Zhou, S., Huang, Z., Wang, Y., Yang, C., He, Y., Yu, J., Yang, P., et al.: Lavie: High-quality video generation with cascaded latent diffusion models. *International Journal of Computer Vision* **133**(5), 3059–3078 (2025)
- [46] Zeng, Y., Wei, G., Zheng, J., Zou, J., Wei, Y., Zhang, Y., Li, H.: Make pixels dance: High-dynamic video generation. In: Proceedings of the IEEE/CVF Conference on Computer Vision and Pattern Recognition, pp. 8850–8860 (2024)
- [47] Ma, Y., Feng, K., Hu, Z., Wang, X., Wang, Y., Zheng, M., He, X., Zhu, C., Liu, H., He, Y., et al.: Controllable video generation: A survey. arXiv preprint arXiv:2507.16869 (2025)
- [48] Hao, Z., Huang, X., Belongie, S.: Controllable video generation with sparse trajectories. In: Proceedings of the IEEE Conference on Computer Vision and Pattern Recognition, pp. 7854–7863 (2018)
- [49] Hu, Y., Luo, C., Chen, Z.: Make it move: controllable image-to-video generation with text descriptions. In: Proceedings of the IEEE/CVF Conference on Computer Vision and Pattern Recognition, pp. 18219–18228 (2022)
- [50] Shi, X., Huang, Z., Wang, F.-Y., Bian, W., Li, D., Zhang, Y., Zhang, M., Cheung, K.C., See, S., Qin, H., et al.: Motion-i2v: Consistent and controllable image-to-video generation with explicit motion modeling. In: ACM SIGGRAPH 2024 Conference Papers, pp. 1–11 (2024)
- [51] Li, C., Huang, D., Lu, Z., Xiao, Y., Pei, Q., Bai, L.: A survey on long video generation: Challenges, methods, and prospects. arXiv preprint arXiv:2403.16407 (2024)
- [52] Ge, S., Hayes, T., Yang, H., Yin, X., Pang, G., Jacobs, D., Huang, J.-B., Parikh, D.: Long video generation with time-agnostic vqgan and time-sensitive transformer. In: European Conference on Computer Vision, pp. 102–118 (2022). Springer
- [53] Henschel, R., Khachatryan, L., Poghosyan, H., Hayrapetyan, D., Tadevosyan, V., Wang, Z., Navasardyan, S., Shi, H.: Streamingt2v: Consistent, dynamic, and extendable long video generation from text. In: Proceedings of the Computer Vision and Pattern Recognition Conference, pp. 2568–2577 (2025)
- [54] Lu, Y., Liang, Y., Zhu, L., Yang, Y.: Free-long: Training-free long video generation with spectralblend temporal attention. *Advances in Neural Information Processing Systems* **37**, 131434–131455 (2024)
- [55] Zhan, C., Li, W., Shen, C., Zhang, J., Wu, S., Zhang, H.: Bidirectional sparse attention for faster video diffusion training. arXiv preprint arXiv:2509.01085 (2025)
- [56] Xing, Z., Dai, Q., Hu, H., Wu, Z., Jiang, Y.-G.: Simda: Simple diffusion adapter for efficient video generation. In: Proceedings of the IEEE/CVF Conference on Computer

- Vision and Pattern Recognition, pp. 7827–7839 (2024)
- [57] Hu, Z., Xu, D.: Videocontrolnet: A motion-guided video-to-video translation framework by using diffusion model with controlnet. arXiv preprint arXiv:2307.14073 (2023)
- [58] Cai, S., Yang, C., Zhang, L., Guo, Y., Xiao, J., Yang, Z., Xu, Y., Yang, Z., Yuille, A., Guibas, L., et al.: Mixture of contexts for long video generation. arXiv preprint arXiv:2508.21058 (2025)
- [59] Wang, Z., Lu, C., Wang, Y., Bao, F., Li, C., Su, H., Zhu, J.: Prolificdreamer: High-fidelity and diverse text-to-3d generation with variational score distillation. *Advances in neural information processing systems* **36**, 8406–8441 (2023)
- [60] Xu, D., Jiang, Y., Wang, P., Fan, Z., Wang, Y., Wang, Z.: Neurallift-360: Lifting an in-the-wild 2d photo to a 3d object with 360deg views. In: *Proceedings of the IEEE/CVF Conference on Computer Vision and Pattern Recognition*, pp. 4479–4489 (2023)
- [61] Tang, J., Wang, T., Zhang, B., Zhang, T., Yi, R., Ma, L., Chen, D.: Make-it-3d: High-fidelity 3d creation from a single image with diffusion prior. In: *Proceedings of the IEEE/CVF International Conference on Computer Vision*, pp. 22819–22829 (2023)
- [62] Deitke, M., Schwenk, D., Salvador, J., Weihs, L., Michel, O., VanderBilt, E., Schmidt, L., Ehsani, K., Kembhavi, A., Farhadi, A.: Objaverse: A universe of annotated 3d objects. In: *Proceedings of the IEEE/CVF Conference on Computer Vision and Pattern Recognition*, pp. 13142–13153 (2023)
- [63] Xiang, J., Lv, Z., Xu, S., Deng, Y., Wang, R., Zhang, B., Chen, D., Tong, X., Yang, J.: Structured 3d latents for scalable and versatile 3d generation. In: *Proceedings of the Computer Vision and Pattern Recognition Conference*, pp. 21469–21480 (2025)
- [64] Liu, R., Wu, R., Van Hoorick, B., Tokmakov, P., Zakharov, S., Vondrick, C.: Zero-1-to-3: Zero-shot one image to 3d object. In: *Proceedings of the IEEE/CVF International Conference on Computer Vision*, pp. 9298–9309 (2023)
- [65] Liu, M., Xu, C., Jin, H., Chen, L., Varma T, M., Xu, Z., Su, H.: One-2-3-45: Any single image to 3d mesh in 45 seconds without per-shape optimization. *Advances in Neural Information Processing Systems* **36**, 22226–22246 (2023)
- [66] Liu, M., Shi, R., Chen, L., Zhang, Z., Xu, C., Wei, X., Chen, H., Zeng, C., Gu, J., Su, H.: One-2-3-45++: Fast single image to 3d objects with consistent multi-view generation and 3d diffusion. In: *Proceedings of the IEEE/CVF Conference on Computer Vision and Pattern Recognition*, pp. 10072–10083 (2024)
- [67] Long, X., Guo, Y.-C., Lin, C., Liu, Y., Dou, Z., Liu, L., Ma, Y., Zhang, S.-H., Habermann, M., Theobalt, C., et al.: Wonder3d: Single image to 3d using cross-domain diffusion. In: *Proceedings of the IEEE/CVF Conference on Computer Vision and Pattern Recognition*, pp. 9970–9980 (2024)
- [68] Yu, H.-X., Duan, H., Hur, J., Sargent, K., Rubinstein, M., Freeman, W.T., Cole, F., Sun, D., Snavely, N., Wu, J., et al.: Wonderjourney: Going from anywhere to everywhere. In: *Proceedings of the IEEE/CVF Conference on Computer Vision and Pattern Recognition*, pp. 6658–6667 (2024)
- [69] Chung, J., Lee, S., Nam, H., Lee, J., Lee, K.M.: Luciddreamer: Domain-free generation of 3d gaussian splatting scenes. arXiv preprint arXiv:2311.13384 (2023)
- [70] Yu, H.-X., Duan, H., Herrmann, C., Freeman, W.T., Wu, J.: Wonderworld: Interactive 3d scene generation from a single image. In: *Proceedings of the Computer Vision and Pattern Recognition Conference*, pp. 5916–5926 (2025)
- [71] Ni, C., Wang, X., Zhu, Z., Wang, W., Li, H., Zhao, G., Li, J., Qin, W., Huang, G.,

- Mei, W.: Wonderturbo: Generating interactive 3d world in 0.72 seconds. arXiv preprint arXiv:2504.02261 (2025)
- [72] Chen, L., Zhou, Z., Zhao, M., Wang, Y., Zhang, G., Huang, W., Sun, H., Wen, J.-R., Li, C.: Flexworld: Progressively expanding 3d scenes for flexible-view synthesis. arXiv preprint arXiv:2503.13265 (2025)
- [73] Popov, S., Raj, A., Krainin, M., Li, Y., Freeman, W.T., Rubinstein, M.: Camctrl3d: Single-image scene exploration with precise 3d camera control. In: 2025 International Conference on 3D Vision (3DV), pp. 649–658 (2025). IEEE
- [74] Ren, X., Shen, T., Huang, J., Ling, H., Lu, Y., Nimier-David, M., Müller, T., Keller, A., Fidler, S., Gao, J.: Gen3c: 3d-informed world-consistent video generation with precise camera control. In: Proceedings of the Computer Vision and Pattern Recognition Conference, pp. 6121–6132 (2025)
- [75] Wang, S., Leroy, V., Cabon, Y., Chidlovskii, B., Revaud, J.: Dust3r: Geometric 3d vision made easy. In: Proceedings of the IEEE/CVF Conference on Computer Vision and Pattern Recognition, pp. 20697–20709 (2024)
- [76] Ho, J., Jain, A., Abbeel, P.: Denoising diffusion probabilistic models. *Advances in neural information processing systems* **33**, 6840–6851 (2020)
- [77] Ho, J., Salimans, T., Gritsenko, A., Chan, W., Norouzi, M., Fleet, D.J.: Video diffusion models. *Advances in neural information processing systems* **35**, 8633–8646 (2022)
- [78] Rombach, R., Blattmann, A., Lorenz, D., Esser, P., Ommer, B.: High-resolution image synthesis with latent diffusion models. In: Proceedings of the IEEE/CVF Conference on Computer Vision and Pattern Recognition, pp. 10684–10695 (2022)
- [79] Ma, B., Gao, H., Deng, H., Luo, Z., Huang, T., Tang, L., Wang, X.: You see it, you got it: Learning 3d creation on pose-free videos at scale. In: Proceedings of the Computer Vision and Pattern Recognition Conference, pp. 2016–2029 (2025)
- [80] Ling, L., Sheng, Y., Tu, Z., Zhao, W., Xin, C., Wan, K., Yu, L., Guo, Q., Yu, Z., Lu, Y., *et al.*: D13dv-10k: A large-scale scene dataset for deep learning-based 3d vision. In: Proceedings of the IEEE/CVF Conference on Computer Vision and Pattern Recognition, pp. 22160–22169 (2024)
- [81] Zhou, T., Tucker, R., Flynn, J., Fyffe, G., Snavely, N.: Stereo magnification: Learning view synthesis using multiplane images. arXiv preprint arXiv:1805.09817 (2018)
- [82] YU, M., Hu, W., Xing, J., Shan, Y.: Trajectorycrafter: Redirecting camera trajectory for monocular videos via diffusion models. arXiv preprint arXiv:2503.05638 (2025)
- [83] Wu, H., Zhang, Z., Zhang, W., Chen, C., Liao, L., Li, C., Gao, Y., Wang, A., Zhang, E., Sun, W., *et al.*: Q-align: Teaching llms for visual scoring via discrete text-defined levels. arXiv preprint arXiv:2312.17090 (2023)
- [84] Yang, Z., Teng, J., Zheng, W., Ding, M., Huang, S., Xu, J., Yang, Y., Hong, W., Zhang, X., Feng, G., *et al.*: Cogvideox: Text-to-video diffusion models with an expert transformer. arXiv preprint arXiv:2408.06072 (2024)
- [85] Wang, J., Chen, M., Karaev, N., Vedaldi, A., Ruppert, C., Novotny, D.: Vggt: Visual geometry grounded transformer. In: Proceedings of the Computer Vision and Pattern Recognition Conference, pp. 5294–5306 (2025)
- [86] Chen, S., Guo, H., Zhu, S., Zhang, F., Huang, Z., Feng, J., Kang, B.: Video depth anything: Consistent depth estimation for super-long videos. In: Proceedings of the Computer Vision and Pattern Recognition Conference, pp. 22831–22840 (2025)
- [87] Yang, L., Kang, B., Huang, Z., Zhao, Z., Xu, X., Feng, J., Zhao, H.: Depth anything v2. *Advances in Neural Information Processing Systems* **37**, 21875–21911 (2024)